Article

Incorporation and deposition of spin crossover materials into and onto electrospun nanofibers

Maximilian Seydi Kilic [1], Jules Brehme [1,2,3], Justus Pawlak [1,3], Kevin Tran [1,3], Takuya Shiga [4], Taisei Suzuki [4], Masayuki Nihei [4], Ralf Franz Sindelar [2,3] and Franz Renz[1,3,*]

[1] Institute of inorganic Chemistry, Leibniz Universität Hannover, Callinstraße 7, 30167 Hannover, Germany maximilian.kilic@acd.uni-hannover.de
[2] Faculty II, Hochschule Hannover, University of Applied Science an Arts, Ricklinger Stadtweg 120, D-30459 Hannover, Germany jules.brehme@hs-hannover.de
[3] Hannover School for Nanotechnology, Laboratorium für Nano- und Quantenengineering (LNQE), Leibniz Universität Hannover, Scheiderberg 39, 30167 Hannover, Germany
[4] Graduate School of Pure and Applied Sciences, University of Tsukuba, Tennodai 1-1-1, Tsukuba, Ibaraki 305-8577, Japan
* Correspondence: franz.renz@acd.uni-hannover.de

Abstract: We synthesized iron(II)-triazole spin crossover compounds of the type $[Fe(atrz)_3]X_2$ and incorporated and deposited them on electrospun polymer nanofibers. In view of possible applications, we chose iron(II)-triazole-complexes that are known to exhibit spin crossover close to ambient temperature. Therefore we used the complexes $[Fe(atrz)_3]Cl_2$ and $[Fe(atrz)_3](2ns)_2$ (2ns = 2-Naphthalenesulfonate) and analyzed them with IR-, UV/Vis and Mossbauer spectroscopy and with a SQUID magnetometer. The synthesized complexes were then in one attempt deposited on fibers of polymethylmethacrylate (PMMA) and in another attempt incorporated into core-shell like PMMA fiber structures. This was done via two different electrospinning methods. Deposition was performed by uniaxial electrospinning and incorporation was performed by coaxial electrospinning. The obtained polymer-complex-composites were then further investitgated by the same methods as the pure complexes as well as by SEM pictures and EDX measurements. The analysis by UV/Vis spectroscopy, Mössbauer spectroscopy and temperature-depended magnetic measurements with the SQUID magnetometer showed that the spin crossover properties were maintained and were not changed after the electrospinning processes and that the complexes were not harmed during the procedure.

Keywords: Spin Crossover, (Coaxial)-electrospinning, Triazole Complexes, nano fibers, PMMA, Coordination Chemistry, Composites

1. Introduction

The reversible transition between high-spin (HS) and low-spin (LS) states can occur in the octahedral ligand field of metal coordination compounds of elements with electron configurations from $3d^4$ to $3d^7$. This transition is known as spin crossover and is triggered by external stimuli like temperature, pressure, guest molecules or chemical influences and irradiation. [1-2] Spin Crossover can be seen as a paradigm for the bistability of spin states at a molecular level. [3-4] The Spin crossover phenomenon is accompanied by a variety of property changes. Compounds containing Fe^{II} for example show a switch between para- and diamagnetic behavior. [5] The spin state change is also accompanied by a change of the optical properties, electronic properties, and a change of the metal to ligand bond length. [6] Therefore, spin crossover materials represent a very active field of research. Through the change of properties, they could possibly find applications within mechanical, electronic, photonic, and optical devices. [7-8]

Complexes with Fe^{II} and triazole ligands are known to have suitable ligand field strengths so that SCO effects can be observed. This is also possible for these complexes around ambient temperature and below as well as above. [9-10] When triazole ligands are

Preprints (www.preprints.org) | NOT PEER-REVIEWED | Posted: 21 December 2022 doi:10.20944/preprints202212.0396.v1

used, which are substituted at the 4-position, the ligands and central atoms form one-dimensional coordination chains. Their general form is described by the formula $[Fe(Rtrz)_3]X_2$ with Rtrz being a 4-substituted-1,2,4-triazole ligand and X being a

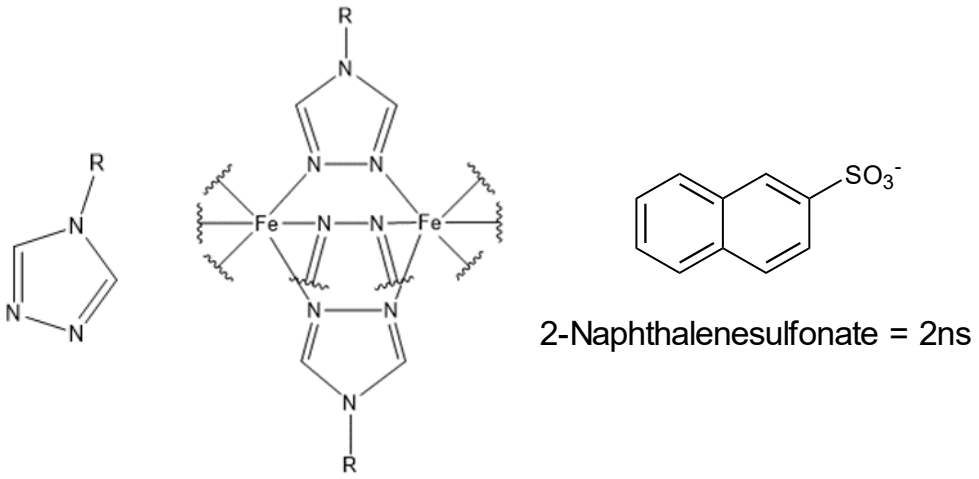

Figure 1. Triazole ligand (left) substituted at the 4-position, schematic illustration of the one-dimensional coordination chains (middle) and the 2ns-anion (right). R refers to any organic rest at the 4-position.

monovalent anion like the chloride- or 2ns-anion. (Figure 1) [8,11] The SCO properties of these coordination chains can be influenced by changing the counterions or changing the substitution of the 4-position. We chose triazole complexes because modification of their SCO properties is possible by simply changing the educts during the synthesis and because they exhibit a high chemical stability. [8,12] This high chemical stability is triggered by triple N^1, N^2-triazole bridges connecting the metal centers in the coordination chains. The reason for the increased chemical stability lies in the bond angles between the metal atoms and the nitrogen of the ligands. These correspond approximately to the exocyclic donor electrons of the five-membered ring, which means that the emerging ring strain is low. [8,10] The high chemical stability is particularly advantageous with regard to the electrospinning process we have been using. In the electrospinning process, the complexes used are subjected to harsh conditions. Electrospinning is a fairly simple technique to produce nanofibers out of polymer solution. In our typical electrospinning process, an electrical potential is applied between a droplet of the solution in a syringe needle and a grounded rotating collector. As soon as the Coulomb forces acting on the droplet overcome the surface tension of the said droplet, a Taylor cone forms, and a fiber jet gets ejected.[13,14]

Previously, we incorporated complexes into polylactic acid (PLA) polymer fibers and showed by Mössbauer spectroscopy that complexes and their SCO properties can be maintained during the electrospinning process for those polymer fibers and the related circumstances. We showed this with complexes that exhibit SCO behavior below room temperature. [15] We now report that the SCO properties also remain after the electrospinning process for triazole complexes that show SCO properties around ambient temperature. Therefore, we synthesized and used the known complexes $[Fe(atrz)_3]Cl_2$ and $[Fe(atrz)_3](2ns)_2$. In addition, the optically active polymer polymethyl methacrylate (PMMA) was used instead of PLA. An optically active material was chosen because of the possibility to use the obtained fibers as part of sensors. Through the controlled implementation of SCO particles into optically active polymer-based fibers a simple and targeted addressing of SCO compounds could be possible. We were now also able to determine the position of the complex particles inside of the complex polymer composite by using SEM pictures and EDX measurements. Subsequently, we used coaxial electrospinning to add a protective shell to the resulting polymer fibers for one attempt so that the attached complexes cannot be detached from the fibers by mechanical action or

Preprints (www.preprints.org) | NOT PEER-REVIEWED | Posted: 21 December 2022 doi:10.20944/preprints202212.0396.v1

water contact. Therefore, we report that the coaxial electrospinning approach resulted in core-shell-like structures with composite as core material and an additional shell of PMMA. Coaxial electrospinning was firstly introduced in 2002 enabling a wider application range for nanofibers and diversifying their morphology. [16] Especially non-polymeric materials (ceramics, metal oxides or semiconducting materials) could be used in the electrospinning process. However, it comes to a price of an increased number of parameters to be taken care of, including shell-to-core fluid flowrate miscibility and compatibility. Since then the coaxial method has been the base for more multichannel electrospinning systems (e.g. triaxial, tetraaxial). [17-19] Important to note is that the viscosity of the shell solution has to be higher than that of the core solution as the requirement to form stable core-shell fibers is to overcome the interfacial surface tension between core and shell solution. Additionally, the flowrate of the shell solution needs to be higher than the core solution so that the core remains completely entrained. [20]

2. Materials and Methods

2.1. General

The used Fe^{II}-triazole complexes and composite materials were synthesized by using the following purchased chemicals without further purifying them: Iron(II)Chloride tetrahydrate ($FeCl_2 \cdot 4\ H_2O$) (>99,0 %) from Sigma-Aldrich, L-ascorbic acid (>99%) from Carl Roth, 4-Amino-1,2,4-Triazole (99 %), purchased from Thermo Scientific, Sodium 2-Naphthalenesulfonate (98 %) from Alfa Aesar, PMMA 350.000 Mw from SigmaAldrich and 2,2,2-Trifluorethanol (TFE) from Carl Roth. The measured Mössbauer spectra were recorded in transmission and ^{57}Co/Rh source was used.

2.2. Synthesis of [Fe(atrz)$_3$]Cl$_2$

A modified synthesis that was based on a synthesis by Bousseksou et al. [21] was performed. Therefore, 0,5887 g of $FeCl_2 \cdot 4\ H_2O$ were dissolved in 1,25 mL H_2O with 20 mg of L-ascorbic acid. Separately 0,746 g 4-Amino-1,2,4-Triazole were dissolved in 1,25 mL H_2O. The iron solution was added to the triazole solution and the resulting solution was stirred for 2 hours. A white solid was obtained in the process. The solid was then further purified by dispersing it in ethanol followed by centrifugation at 6000 rpm for 10 min for 3 times. In the process, the solid changed color from white to pink. The product was subsequently dried in the air and 1,08 g were obtained. (Yield: 85 %). Analytically found (calculated) with CNH elemental analysis for $C_6H_{12}N_{12}Cl_2 \cdot 2{,}85H_2O$ (molar mass 430,33 g mol^{-1}): C, 16,91 (16,75); H, 3,47 (4,15); N, 38,98 (39,06). Far-infrared (FIR) (in cm^{-1}): 469 (w), 479 (w), 515 (w), Mid-Infrared (MIR) (in cm^{-1}): 623 (s), 701 (s), 852 (w), 869 (m), 891 (m), 1001 (m), 1031 (w), 1063 (m), 1100 (s), 1219 (s), 1313 (w), 1357 (w), 1401 (w), 1486 (w), 1543 (m), 1618 (s), 1663 (s), 3014 (w), 3081 (m), 3113 (s), 3197 (m), 3265 (s), 3301 (s), 3400 (s).

2.3. Synthesis of [Fe(atrz)$_3$](2ns)$_2$

First, the corresponding iron(II) salt had to be obtained based on a synthesis by Caseri et al [22], then the complex was synthesized also following the modified synthesis by Bousseksou et al. [21] Therefore, to obtain $Fe(2ns)_2 \cdot 6\ H_2O$, 2,5 g Sodium 2-Naphthalenesulfonate were dissolved in 75 mL H_2O by heating up to 70 °C and stirring at 650 rpm. A dull solution was obtained. Separately 1,08 g of $FeCl_2 \cdot 4\ H_2O$ were dissolved in 2,5 mL H_2O and then added to the Sodium 2-Naphthalenesulfonate solution. A white solid precipitated from the solution, which was then washed 3 times with 150 mL of water. The white solid was then dried in a desiccator under vacuum and 1,9978 g (Yield: 3,45 mmol, 64 %) were obtained. The white precipitate was further analyzed by IR spectroscopy to confirm that $Fe(2ns)_2 \cdot 6\ H_2O$ had been obtained. MIR (in cm^{-1}) : 612 (m), 621 (m), 645 (m), 668 (m), 736 (w, broad), 758 (s), 815 (s), 906 (w), 943 (w), 964 (w), 1033 (s),

Preprints (www.preprints.org) | NOT PEER-REVIEWED | Posted: 21 December 2022 doi:10.20944/preprints202212.0396.v1

1091 (m), 1181 (s, broad), 1347 (w), 1503 (m), 1592 (m), 1646 (s), 1670 (w), 1981 (w), 2364 (w, broad), 3061 (w), 3364 (s, broad).

Then 0,8562 g of the obtained iron(II) salt were dissolved in 4 mL of methanol. Separately 0,373 g 4-Amino-1,2,4-Triazole were dissolved in 3 mL H_2O. The solution of the iron(ii) salt was then added to the 4-Amino-1,2,4-Triazole solution and was stirred for 2 hours. Thereby a pink precipitate was formed. The obtained solid was then purified by dispersing it in ethanol and centrifuging it 3 times at 6000 rpm for 10 min. The obtained solid was then dried in a desiccator and 0,632 g were obtained. (Yield: 0,8245 mmol, 56 %) Analytically found (calculated) with CNH elemental analysis for $C_{26}H_{26}N_{12}O_6S_2 \cdot 2{,}44H_2O$ (molar mass 766,49 g mol^{-1}): C, 40,55 (40,74); H, 3,67 (4,06); N, 21,77 (21,93). FIR (in cm^{-1}): 474 (m), 502 (m), 552 (s), 560 (s), 568 (s), 622 (s), 647 (m), 675 (s), 748 (s), 768 (w), 819 (s), 865 (s), 906 (s), 944 (m), 956 (m), 981 (w), 1032 (s), 1063 (m), 1093 (s), 1138 (s), 1184 (s), 1271 (s), 1346 (w), 1383 (w), 1446 (m), 1504 (w), 1544 (w), 1593 (w), 1628 (m, broad), 3011 (w), 3060 (m), 3073 (w), 3134 (w), 3163 (m), 3214 (w), 3283 (m, broad), 3498 (m, broad).

2.4. Electrospinning of PMMA fibers with $[Fe(atrz)_3]Cl_2$

A solution was prepared dispersing 0,227 g $[Fe(atrz)_3]Cl_2$ in 10 mL TFE (2,2,2-Trifluoroethanol) and sonicating the solution for 1h. then 1,35 g PMMA were added to the solution and it was stirred overnight for 12 h to obtain a homogeneous solution. The mixture was the electrospun at 18 kV, with a pumping rate of 1 ml/h, with a collector speed of 10 m/s and the polymer complex composite (PCC) collected on an aluminum foil, as schematically shown in Figure 2.

2.5. Coaxial Spinning of PMMA fibers with $[Fe(atrz)_3](2ns)_2$

For the shell solution, 1,5 g PMMA were dissolved in 10 mL TFE and stirred overnight for 12h to obtain a homogenous solution. The core solution contained 500 mg of $[Fe(atrz)_3](2ns)_2$ which was dispersed in 10ml TFE and sonicated for 1h to gain unisized particles before 0,5 g PMMA was added to the solution. Following that the solution was

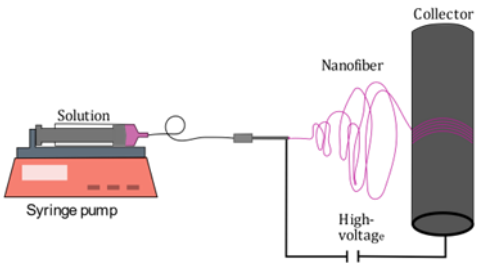

Figure 2. Deposition of $[Fe(atrz)_3]Cl_2$ onto PMMA nanofibers via electrospinning. During the emersion of the fiber jet the solvent evaporates so that the solid polymer-complex nanofiber composite can be collected, using the rotating drum collector for further fiber aligment.

stirred overnight for 12 h to obtain a homogenous solution. Those mixtures were electrospun at 18 kV, 1,3 ml/h for the shell and 0,9 ml/h for the core with a collector speed of 10 m/s while the fibers were collected on an aluminum foil, as pictured in Figure 3.

Preprints (www.preprints.org) | NOT PEER-REVIEWED | Posted: 21 December 2022 doi:10.20944/preprints202212.0396.v1

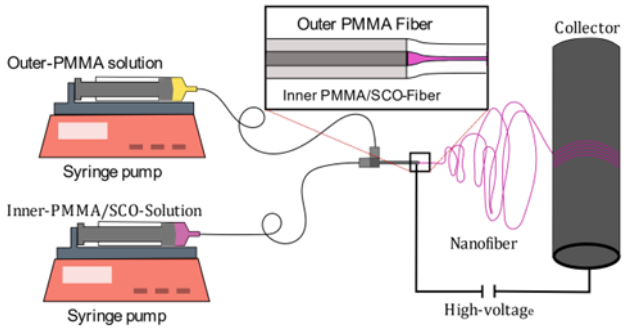

Figure 3. Implementation of $[Fe(atrz)_3](2ns)_2$ into PMMA nanofibers via coaxial electrospinning. The outer solution drags the inner solution with it to the collector, leading to the need of a higher pump rate of the outer solution. For fiber depletion the same effect takes places as for the previous electrospinning process.

3. Results

3.1. Electrospun PMMA nanofibers with $[Fe(atrz)_3]Cl_2$

Through the uniaxial electrospinning process, we obtained a pink-colored fiber mat. In Figure 4a) the IR-Spectrum of the composite product in which the complex shall be deposited outer surface of the fibers is shown. This is shown in comparison to the IR-spectra the pure PMMA nanofibers and the pure complex. The C=O band at 1750 cm^{-1} is clearly assignable to the PMMA as there are none in the ligands of the complex. Through the comparison, it can be seen that some of the most important bands of both the pure PMMA nanofibers and the complex are still visible in the composite product. The bands also show no shift in their wavenumber, indicating no chemical interaction between the complex and the nanofibers. Which lead us to the assumption that the complex was still present after the electrospinning process and did not surcome to the harsh conditions of the spinning process. Due to the ratio of complex to polymer the bonds of the polymer are overlapping the bonds of the complex. Especially the weaker bonds seem to be overshadowed by the polymer bonds. Nevertheless, it can be seen in the fingerprint area that some triazole bonds are still visible and can't be assigned otherwise to the polymer.

As further proof that the complex is inside the composite product a Mossbauer spectrum at ambient temperature was measured. The Mossbauer spectrum which is shown in figure 4b) shows the presence of iron(II). Therefore, it can be said that next to the polymer the complex must be present. That the complex is neither oxidized nor decomposed through the electrospinning process can be assumed due to the measured isomeric shift ($\delta = 0.424$ mm s^{-1}) and the occuring small quadrupol splitting ($\Delta E_Q = 0.172$ mm s^{-1}) that can be observed in the spectrum, which is in the common range for iron(II) triazole complexes in the LS-state. [15, 23]

Preprints (www.preprints.org) | NOT PEER-REVIEWED | Posted: 21 December 2022 doi:10.20944/preprints202212.0396.v1

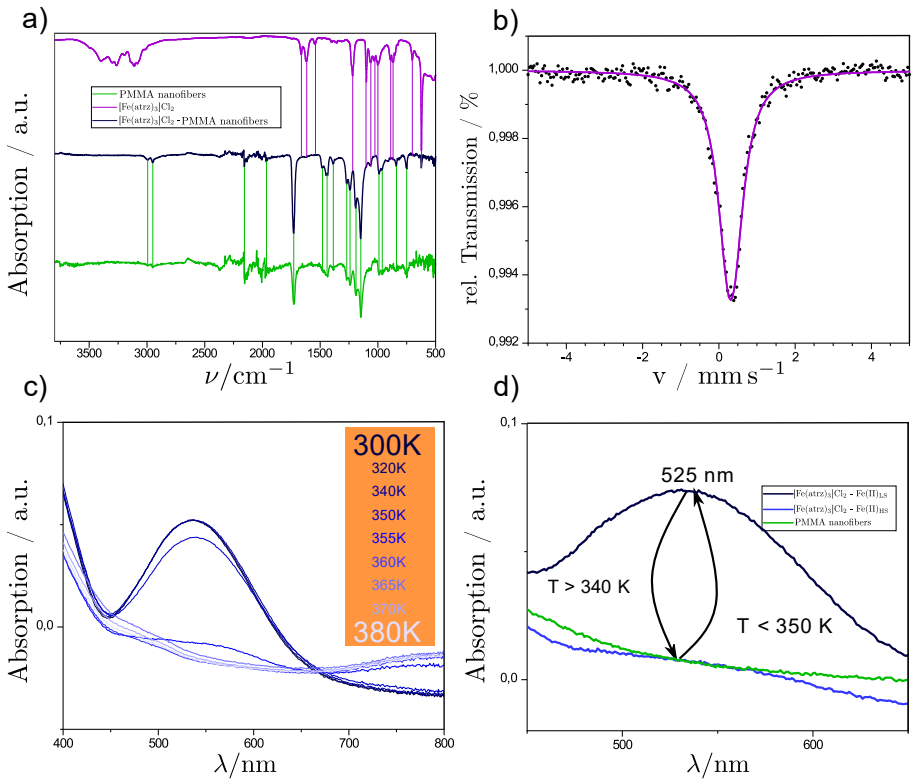

Figure 4. a) Comparison of the IR-Spectra of the pure PMMA fibers, the pure complex $[Fe(atrz)_3]Cl_2$ and the fiber complex composite. It is visible that the fcc spectra contain the sharpest, most defining bonds from both the complex, such as the triazole bonds and fiber, such as acrylate bond, amplifying our claim of the successful synthesis of that composite. b) Mossbauer spectrum of $[Fe(atrz)_3]Cl_2$ deposited on PMMA nano fibers at room temperature. Showing that no oxidation occurred during the electrospinning process and that the iron(II) remained in the LS State. c) As the band at 525nm diminishes the composites changes its colour from a dark pinkish tone to white, which can be seen as proof of the successful spin state switch and the maintaining of the SCO properties after the electrospinning process. As the temperature rises the amount of the Fe(II) from the $[Fe(atrz)_3]Cl_2$ in the HS state continuous to rise up till all Fe is in the HS state. D) Complete UV/Vis spectro of $[Fe(atrz)_3]Cl_2$ on the PMMA fiber and the destinc colorgiving part at 525nm. We show that the spin transition still occurs at the typical temperature.

As the Mossbauer analysis showed us that iron was present in the composite, UV/Vis measurements were done to investigate the spin crossover properties as a color change occurs during the spin state switch from pink to white. In Figure 4d) is a comparison of pure PMMA nanofibers with polymer-complex-composites (PCC) in the LS and HS-state. In the range between 450 and 650 nm a peak at 525 nm occurs at room temperature when the complex is in the low spin state according to the Mossbauer spectrum. This peak represents the color-giving band, as it is the only one in the spectrum of the visible light. As we increased the temperature, we observed a decrease in the absorption of said band. After reaching a certain temperature no further decrease was observed. Which has to be connected to the characteristic color change of iron(II)-triazole complexes from pink to white. Therefore, the spin crossover occurred during the heating process where the complex changes its spin state to HS.

Preprints (www.preprints.org) | NOT PEER-REVIEWED | Posted: 21 December 2022 doi:10.20944/preprints202212.0396.v1

To further analyse the switching behaviour of the complex and the PCC, magnetic measurements with a SQUID magnetometer were performed. The measurements in figure 5 also showed that the SCO behaviour maintained with only a slight change of the occurring hysteresis. It was possible for the measurement of the pure complex $[Fe(atrz)_3]Cl_2$ to be illustrated by the molar magnetic susceptibility in dependence of the applied temperature. For the case of PCC the dependence of the magnetic moment of the composite in emu from the temperature is depicted, as it is also possible to depict the hysteresis in this way. The value for $T_{1/2}\downarrow$of the complex could be found at ~342 K and the $T_{1/2}\uparrow$value at ~350 K. The PCC in comparison showed a $T_{1/2}\downarrow$ value at ~345 K and a $T_{1/2}\uparrow$value at ~353 K. Therefore, no notable change to the hysteresis occurred after the electrospinning process but a slide shift of the switching temperature was observed.

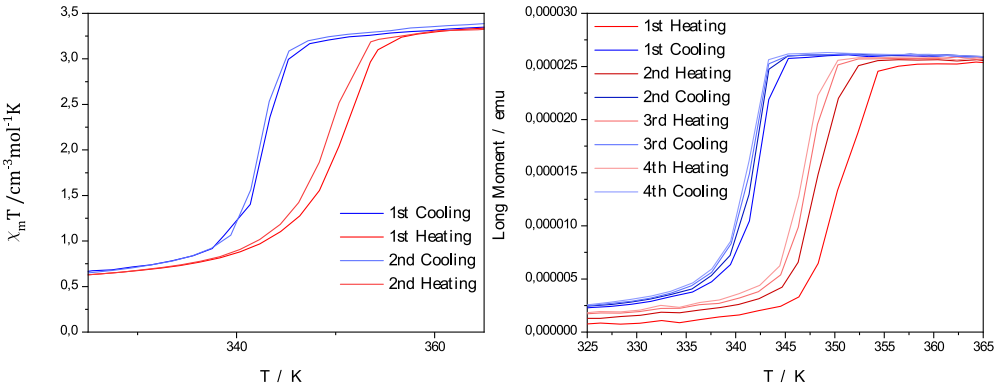

Figure 5 Magnetic measurements performed with a SQUID-magnetometer. Pure complex $[Fe(atrz)_3]Cl_2$ shown on the left described by the magnetic susceptibility in dependence of the temperature. The $T_{1/2}\uparrow$ value is at ~350 K and $T_{1/2}\downarrow$ at ~342 K. PCC on the right represented by magnetic moment in dependence of the temperature. The $T_{1/2}\uparrow$ value is at ~353 K and $T_{1/2}\downarrow$ at ~345 K. The width of the hysteresis remains the same, as it is just shifted to a slightly higher temperature.

Through the IR-Spectrum and the Mossbauer-Spectrum we were able to show that the complex was present and not harmed after the electrospinning process and the UV-Vis spectrum and the SQUID-measurement showed the SCO properties still remained. Through SEM pictures and EDX measurements which are shown in figure 6 we were also able to determine the position of the particles in the product which we obtained through the uniaxial electrospinning process. Through the SEM pictures we could estimate that the complex was deposited on the surface of the obtained nanofibers as cloth-like structures. The average nanofiber diameter was around 250 to 300 nm as measured from the images. Using EDX measurements we investigated those cloths and could prove that the cloths were indeed the used complex. This is visible in figure 6 on the left as the EDX shows a punctual increase of iron at the position of said cloths and also an increase of chlorine as the complex contains iron and chlorine which the PMMA does not.

Preprints (www.preprints.org) | NOT PEER-REVIEWED | Posted: 21 December 2022 doi:10.20944/preprints202212.0396.v1

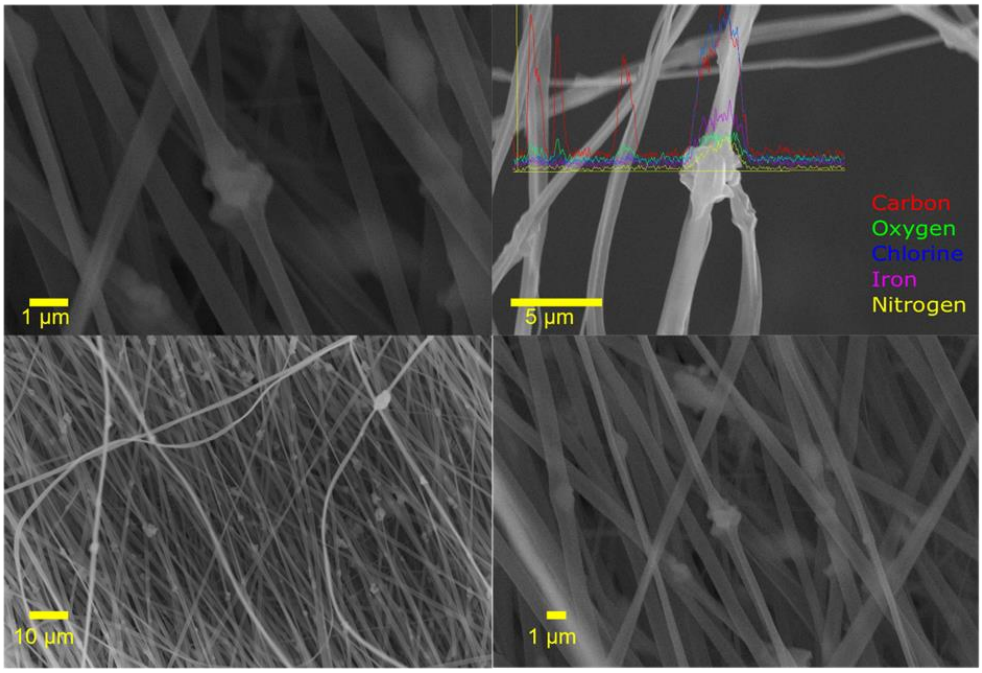

Figure 6. SEM Images of $[Fe(atrz)_3]Cl_2$ nanofiber composit. The little cloths of Complex are well distributed onto the surface of the PMMA nano fibers leading to the unicolor fiber mat that is observable, as no darker or lighter spots could be seen while examining the complex fiber composit mat. SEM-EDX measurement of $[Fe(atrz)_3]Cl_2$ on a cut through 4 fibers. The results indicate that the position of the complex is on the polymer fiber as small points/clots on the fibers. The pure fiber has only Carbon and Oxygen as detected elements as expected, while the complex has clear Chlorine Iron and Nitrogen are detected.

3.2. Coaxial electruspun PMMA nanofibers with $[Fe(atrz)_3](2ns)_2$

We obtained a pink-colored fiber mat using the coaxial electrospinning process like the uniaxial spun nanofiber composite. In Figure 7a) the IR-spectra of pure PMMA fibers, pure complex, and the coaxial spun composite are displayed.

As in this case, the composite contained more complex in the synthesis, the intensity of the bands is more visible. Again, the C=O band at 1700 cm^{-1} is clearly assignable to the PMMA, and some of the most important bands of the complex are visible in the composite. This leads to the same conclusion that the complex is still present, and did not surcome to the conditions of the electrospinning process.

A Mossbauer spectrum at room temperature was also in this case measured to prove that the obtained composite product contained the used complex and that the complex was not decomposed. The spectrum which is shown in figure 7b) indicates the presence of iron(II) in the LS-State with a typical isomeric shift ($\delta = 0.256$ mm s^{-1}) and quadrupol splitting ($\Delta E_Q = 0.361$ mm s^{-1}) for iron(II) triazole complexes in this spin state. [15, 23] Therefore, it can be stated that this complex was also not oxidized or decomposed during the electrospinning process.

Preprints (www.preprints.org) | NOT PEER-REVIEWED | Posted: 21 December 2022 doi:10.20944/preprints202212.0396.v1

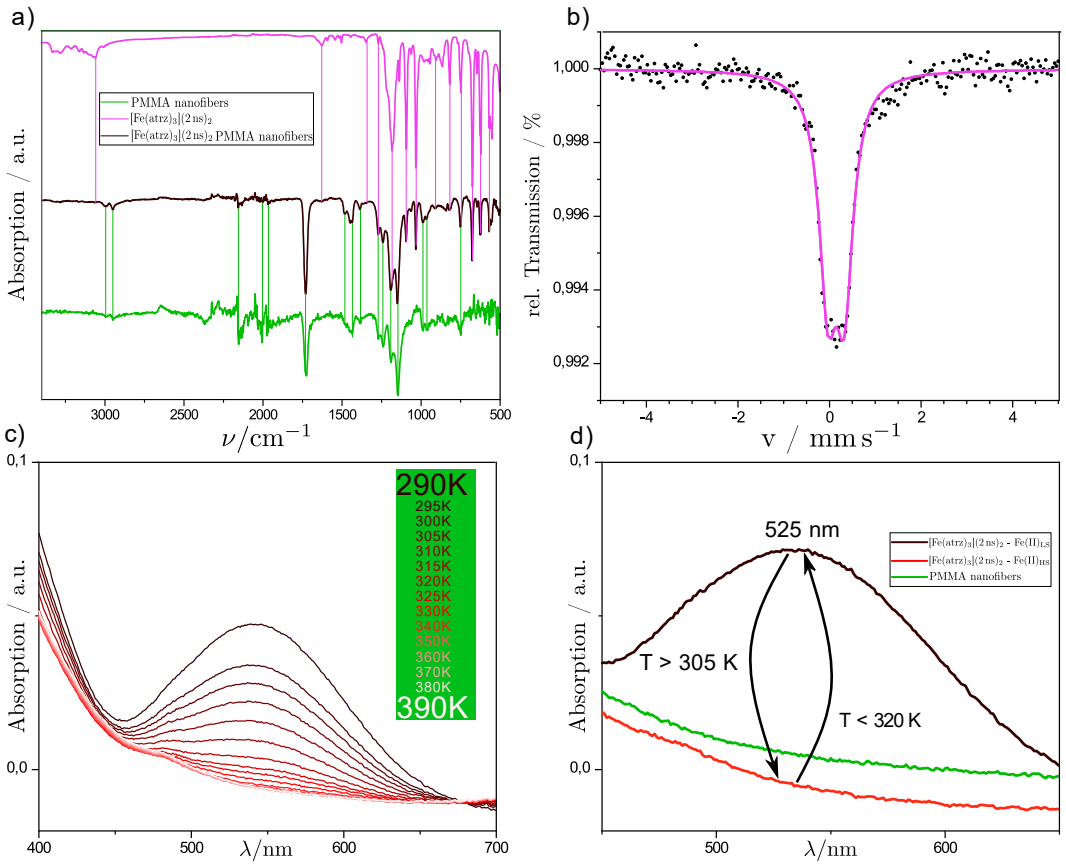

Figure 7. a) Comparison of the IR-Spectra of the pure PMMA fibers, the pure complex $[Fe(atrz)_3](2ns)_2$ and the fiber complex composite. It is visible that the fcc spectra contains the sharpest, most defining bonds from both the complex, such as the triazole bonds and fiber, such as acrylate bond, amplifying our claim of the successful synthesis of that composite. b) $[Fe(atrz)_3](2ns)_2$ was also not oxidized after the implementation into PMMA nano fibers and remained in the LS state. c) As the band at 525 nm diminishes the composites changes its colour from a light pinkish tone to white, which can be seen as a proof of the succesfull spin state switch and the maintaining of the SCO properties after the electrospinning process. As the temperature rises the amount of the Fe(II) from the $[Fe(atrz)_3](2ns)_2$ in the HS state continuous to rise up till all Fe is in the HS state. D) The Fibers were placed at the Ulbricht sphere, as that allowed to measure in absorption and additionally made it possible to use a Peltier element to continously heat up the sample by ramping the voltage up to 6 V at 3 A, and reaching a temperature of maximum 373 K to guarantee all of the Fe(II) from the complex indeed changed its's spin state from LS to the HS state. A difference of the bond at 525 nm is also visible in comparison to the pure PMMA nanofiber without deposited complex.

The through Mossbauer analysis gained information, that Iron(II) was present in the composite, UV/VIS measurements were performed to investigate the spin crossover properties as previously done for the uniaxial spun composite. In Figure 7d) comparison of pure PMMA fibers and coaxial spun composite fibers at room temperature and high temperature is shown. Additionally, multiple UV/Vis spectra were done for different temperatures, as we increased the potential of the used Peltier element. In these UV/Vis measurements it was visible that a bond at 525 nm diminished with increasing the temperature. This behaviour can be attributed to the SCO effect and the switching properties of the complex $[Fe(atrz)_3](2ns)_2$. To further analyse the switching properties of the PCC, SQUID magnetometer measurements were performed. The SQUID measurement is depicted in figure 8 and is compared with a SQUID measurement of the pure complex. The magnetic hysteresis curve of the PCC is shown by the magnetic moment in emu in dependence of the temperature. $T_{1/2}\downarrow$for the PCC can be found at ~296 K and $T_{1/2}\uparrow$at ~315 K. The hysteresis curve of the complex is depicted with the molar magnetic susceptibility in dependence of the temperature. For the complex $T_{1/2}\downarrow$can be

Preprints (www.preprints.org) | NOT PEER-REVIEWED | Posted: 21 December 2022 doi:10.20944/preprints202212.0396.v1

found roughly at ~293 K and $T_{1/2}\uparrow$~317 K indicating a diminishment of the hysteresis due to the implementation of the complex into the poly fiber and a slide shift of the SCO

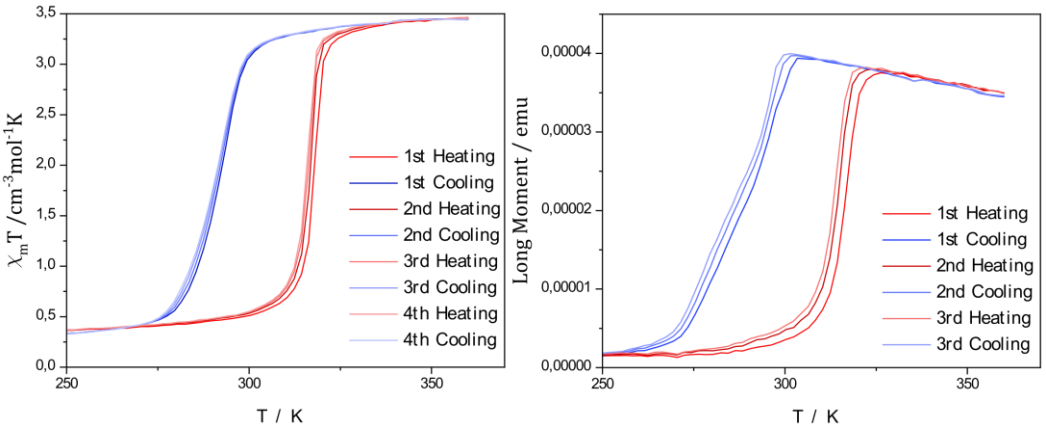

Figure 8. Magnetic measurements performed with a SQUID-magnetometer. Pure complex $[Fe(atrz)_3](2ns)_2$ shown on the left described by the magnetic susceptibility in dependence of the temperature. The $T_{1/2}\uparrow$ value is at ~317 K and $T_{1/2}\downarrow$ at ~293 K. PCC on the right is represented by magnetic moment in dependence of the temperature. The $T_{1/2}\uparrow$ value is at ~315K and $T_{1/2}\downarrow$ at ~296 K. The hysteresis of the PCC is shortened by 5 K in comparison to the pure complex.

The SEM images gave information away how the structure of the nanofibers were. In Figure 7 it can be seen that coaxial nanofibers were successfully made. Additionally, some single nanofibers are visible with a diameter under 100 nm, showing that the coaxial electrospinning process was completely ideal. Nevertheless, the overview shows that the great majority is coaxially spun. To determine the Triazole-complex's possible location, an EDX analysis was performed in one line along the nanofiber. The resulting graph in Figure 9 in the top right indicates the presence of the 2ns in the nanofiber is equally distributed. As the line crosses multiple other nanofibers the EDX measurement has an exceeding amount of more Signals of each element detected as we expected. Of course because of the sheer amount of Carbon and Nitrogen (coming from the PMMA and the triazole-ligand) in the composite, predominantly the two are detected the most.

Preprints (www.preprints.org) | NOT PEER-REVIEWED | Posted: 21 December 2022 doi:10.20944/preprints202212.0396.v1

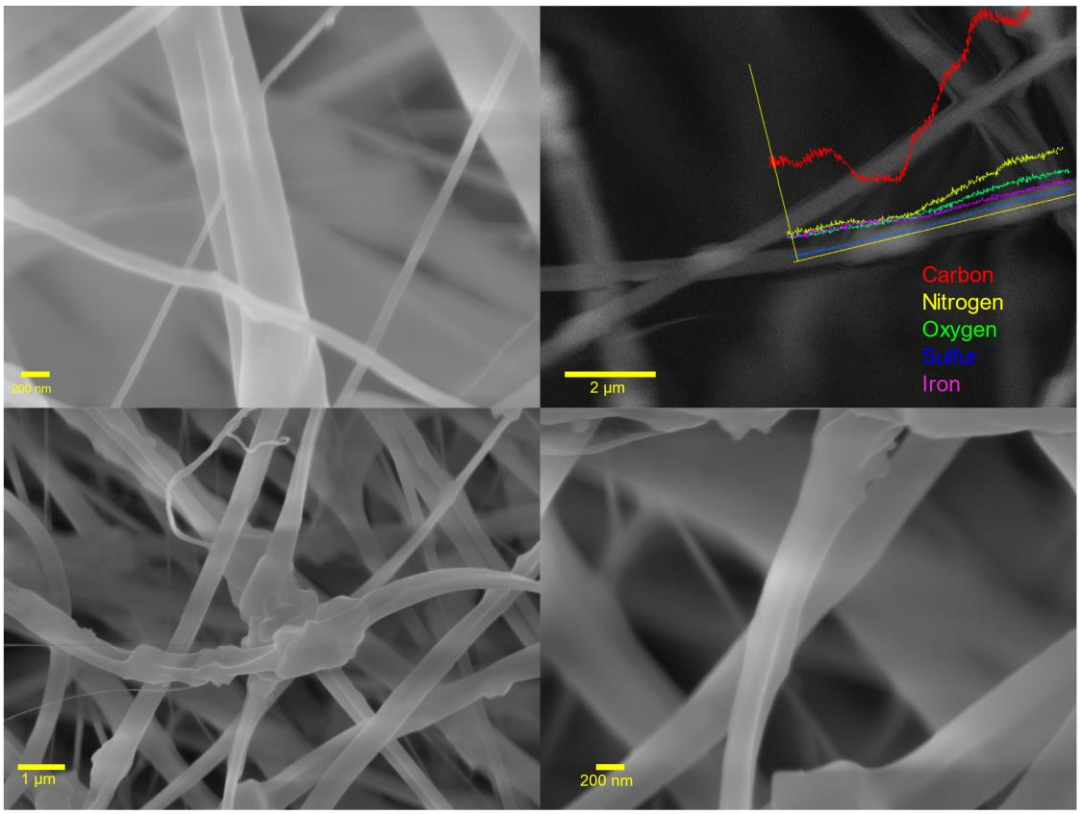

Figure 9. SEM of Coaxial spun complex fiber composit with $[Fe(atrz)_3](2ns)_2$. Althought many fibers are coaxial, still some smaller fiber have emerged forming pure PMMA fiber. Those can happen if during the spinning process a droplet forms at the needle tip leading to a drastic change of the electric field leading to the formation of single fibers without inner solution.

4. Discussion

In this study we present two successful ways of the implementation of Iron-(II)-triazole SCO materials into optical active polymer nanofibers via (coaxial)-electrospinning. The structural integrity of the Iron-Triazole complexes remained intact after the spinning process, which was indicated using Mossbauer- and Infrared-spectroscopy. We were able to maintain the SCO capabilities, proven by temperature dependent UV/Vis spectroscopy as the colour of the material changes from pink to white as the bond at ~525 nm decreased with rising temperature, as well as SQUID measurements with visible hysteresis curves. Additionally, SEM images were taken to determine the morphology and EDX measurements along an one dimensional axis to determine the position of the SCO in the nanofiber structure. As it was intended the SCO is in the inside of the nanofiber structure for the coaxial electrospinning setup, and for the normal electrospinning setup the SCO particles built little cloths with a neat regular distance along the axis on the nanofiber. According to the SQUID measurements this brought a slight difference in the hysteresis as for the coaxial spun PCC said hysteresis diminished by roughly 5 K compared to the pure complex. In comparison, the uniaxial spun PCC showed no change in width regarding the hysteresis. In both cases the SCO temperature was slightly shifted to higher temperatures of roughly 3 K.

This study shows a great starting point to further the application of SCO's into small scale optical fibers and towards a broader range of possible applications. Especially the choice between classic and coaxial electrospinning depending on the application is a great tool as the SCO's can be isolated from chemical influences when inside the fibers as long as the fiber won't get damaged, as the SCO properties are not drastically influenced by the surrounding polymer nanofiber. To switch around in the coaxial setup on the other

hand the SCO would need to be soluble to be placed around the nanofiber, as otherwise it can be expected that the SCO's would simply deplet like in our case for the classic electrospinning process.

Author Contributions: Conceptualization, methodology, validation, formal analysis, writing—original draft preparation, Maximilian Seydi Kilic and Jules Brehme; investigation, Justus Pawlak, Kevin Tran, Takuya Shiga, Taisei Suzuki and Masayuki Nihei; writing—review and editing, Takuya Shiga, Masayuki Nihei, Ralf Sindelar and Franz renz; supervision and project administration, Ralf Sindelar and Franz Renz. All authors have read and agreed to the published version of the manuscript.

Funding: This research received no external funding.

Institutional Review Board Statement: Not applicable.

Data Availability Statement: Link not provided yet.

Acknowledgments: The author would thank the Deutsche Forschungsgemeinschaft (DFG), hannover school for nanotechnology (hsn), Leibniz University Hannover (LUH), University of Tsukuba, Laboratory of Nano and Quantum Engineering (LNQE) and University of Applied Science and Arts (HsH).

Conflicts of Interest: The authors declare no conflict of interest.

References

1. J. E. Angulo-Cervera, M. Piedrahita-Bello, B. Martin, S. E. Alavi, W. Nicolazzi, L. Salmon, G. Molnár and A. Bousseksou, Mater. Adv., 2022, 3, 5131.
2. Spin Transition in Heteroanion Complexes in the Fe^{2+}-4-Amino-1,2,4-Triazole–NO_3^-–SO_4^{2-} System, K.A. Vinogradova, A. Yu. Andreeva, D. P. Pishchur, M. B. Bushuev, J Struct Chem 61, 1380–1389 (2020).
3. J. A. Real, A. B. Gaspar, M. C. MuÇoz, Dalton Trans. 2005, 2062–2079.
4. P. Gamez, J. S. Costa, M. Quesada, G. Arom , Dalton Trans. 2009, 7485 – 7853
5. P. Gütlich, A. Hauser, H. Spiering, Angew. Chem. 1994, 106, 2109–2141; Angew. Chem. Int. Ed. Engl. 1994, 33, 2024 – 2054.
6. A. Hauser, Top. Curr. Chem., 2004, 233, 49–58.
7. A. Bousseksou, G. Molnár, L. Salmon, W. Nicolazzi, Chem. Soc. Rev. 2011, 40, 3313 – 3335.
8. Roubeau, O. (2012), Triazole-Based One-Dimensional Spin-Crossover Coordination Polymers. Chem. Eur. J., 18: 15230-15244.
9. G. Arom , L. A. Barrios, O. Roubeau, P. Gamez, Coord. Chem. Rev. 2011, 255, 485 – 546
10. J. G. Haasnoot, Coord. Chem. Rev. 2000, 200 – 202, 131 – 185
11. O. Kahn, C. J. Martinez, Science 1998, 279, 44–48
12. Sugahara A, Kamebuchi H, Okazawa A, Enomoto M, Kojima N. Control of Spin-Crossover Phenomena in One-Dimensional Triazole-Coordinated Iron(II) Complexes by Means of Functional Counter Ions. Inorganics. 2017; 5(3):50.
13. P.K. Baumgarten, Electrostatic spinning of acrylic microfibers, Journal of colloid and interface science 1971, 36, 71-79.
14. G.I. Taylor, Electrically driven jets, Proceedings of the Royal Society of London. A. Mathematical and Physical Sciences 1969, 313, 453-475
15. F., Renz, Dreyer, B., Natke, D., Klimke, S. et al. Implementation of spin crossover compounds into electrospun nanofibers. Hyperfine Interact 239, 8 (2018)
16. Z. Sun, E. Zussman, A. L. Yarin, J. H. Wendorff, A. Greiner, Adv. Mater. 2003, 15, 1929-1932
17. Z. Shami, N. Sharifi-Sajani, S. Khoee, R. Faridi-Majidi, Ind. Eng. Chem. Res. 2014, 53, 14963
18. Y. M. Chen., Z. G. Lu, L. M. Zhou, Y.-W. Mai, H. T. Huang, Energy Environ. Sci, 2012, 5, 7898
19. B.-S. Lee, H.-S. Yang, W.-R. Yu, Nanotechnology 2014, 25, 465602
20. J. Yoon, H.S. Yang, B.-S. Lee, W.-R. Yu, Adv. Mater. 2018, 30, 1704765
21. M. Piedrahita-Bello, K. Ridier, M. Mikolasek, G. Molnár, W. Nicolazzi, L. Salmon and A. Bousseksou, Chem. Commun., 2019, 55, 4769
22. Irene Bräunlich, Antoni Sánchez-Ferrer, Matthias Bauer, Rahel Schepper, Philippe Knüsel, Julia Dshemuchadse, Raffaele Mezzenga, and Walter Caseri, Inorganic Chemistry 2014 53 (7), 3546-3557